

Ionization corrections in a multi-phase interstellar medium: Lessons from a $z_{\text{abs}} \sim 2$ sub-DLA.

Nikola Milutinovic¹, Sara L. Ellison¹, J. Xavier Prochaska², Jason Tumlinson³

¹*Department of Physics and Astronomy, University of Victoria, Victoria, B.C., V8P 1A1, Canada*

²*Department of Astronomy and Astrophysics, UCO/Lick Observatory, University of California, 1156 High Street, Santa Cruz, CA 95064, USA*

³*Space Telescope Science Institute, 3700 San Martin Drive, Baltimore, MD 21218, USA*

21 November 2018

ABSTRACT

We present a high resolution (FWHM= 2.7 km s⁻¹), high S/N echelle spectrum for the $z_{\text{em}} = 2.26$ QSO J2123–0050 and determine elemental abundances for the $z_{\text{abs}} = 2.06$ sub-DLA in its line of sight. This high redshift sub-DLA has a complex kinematic structure and harbours detections of neutral (S I, C I), singly (e.g. C II, S II) and multiply ionized (e.g. C IV, Si IV) species as well as molecular H₂ and HD. The plethora of detected transitions in various ionization stages is indicative of a complex multi-phase structure present in this high redshift galaxy. We demonstrate that the ionization corrections in this sub-DLA are significant (up to ~ 0.7 dex). For example, if no ionization correction is applied, a super-solar metallicity is derived ($[S/H] = +0.36$), whereas a single phase ionization correction reduces this to $[S/H] = -0.19$. The theoretical impact of a multi-phase medium is investigated through Cloudy modelling and it is found that the abundances of Si, S and Fe are always over-estimated (by up to 0.15 dex in our experiments) if a single-phase is assumed. Therefore, although Cloudy models improve estimates of metal column densities, the simplification of a single phase medium leaves a systematic error in the result, so that even ionization-corrected abundances may still be too high. Without ionization corrections the properties of this sub-DLA appear to require extreme scenarios of nucleosynthetic origins. After ionization corrections are applied the ISM of this galaxy appears to be similar to some of the sightlines through the Milky Way.

Key words: quasars: absorption lines, galaxies: high redshift

1 INTRODUCTION

The measurement of rest-frame ultra-violet resonance lines in damped Lyman alpha (DLA) systems is currently the most successful technique for determining chemical abundances at high redshift (e.g. Prochaska et al. 2003; Wolfe, Gawiser & Prochaska 2005). The largest compilations of DLA abundances include column densities for over a dozen different elements in some 200 absorbing galaxies (e.g. Prochaska et al. 2007b; Dessauges-Zavadsky et al. 2009). It is usually assumed that, due to the high $N(\text{H I})$ column density of the absorber, ionization corrections are negligible and that total elemental column densities can be derived from the dominant ionization state, i.e. the lowest energy species where the ionization potential is above 13.6 eV. For the majority of elements observed in absorption, such as silicon, iron, zinc, sulphur, nickel, titanium and chromium, this is the singly ionized species, leading to the approximation $N(X) \approx N(X \text{ II})$. Exceptions include oxygen and nitrogen whose first ionization potential is close to that of hydrogen and whose ionization balance is governed by charge exchange so that the neutral atom is the dominant species. Therefore, although absorption from non-dominant species is observed in DLAs (such as C IV, Mg I and Na I) their contributions are minor and not usually

considered in abundance determinations. The robustness of this approach to abundance calculations has been tested numerous times in the literature (Viegas 1995; Howk & Sembach 1999; Vladilo et al. 2001; Prochaska et al. 2002a), usually through models that employ the ionization code Cloudy (Ferland et al. 1998). Although the exact magnitude of the corrections depends on a variety of input parameters, most notably the shape and normalization of the ionizing background (e.g. Viegas 1995; Howk & Sembach 1999), in general the literature agrees that the majority of DLA column densities do not require significant ionization corrections (e.g. Vladilo et al. 2001). However, there are a few noteworthy cases where ionization corrections may be important (Prochaska et al. 2002a; Prochaska et al. 2002b; Dessauges-Zavadsky et al. 2004; Dessauges-Zavadsky et al. 2006; Ellison et al. 2010).

As the column density of neutral hydrogen decreases, the self-shielding approximation becomes less robust as more ionizing photons penetrate the cloud. For example, it has been shown that the ratio of Al III/Al II (or some proxy for Al II if it is saturated) tends to increase as the $N(\text{H I})$ decreases (Vladilo et al. 2001). As studies of quasar absorption line systems began to push down the $N(\text{H I})$

scale to investigate the nature of sub-DLAs¹ with $19.0 < \log N(\text{H I}) < 20.3 \text{ cm}^{-2}$ (e.g. Peroux et al. 2003) it was natural to re-assess the need for ionization corrections (Dessauges-Zavadsky et al. 2003; Meiring et al. 2007). Once again, it was found that, in general, ionization corrections were small (below 0.2 dex) and observed column densities are therefore usually converted directly into metallicities (e.g. Peroux et al. 2007; Dessauges-Zavadsky et al. 2009). Nonetheless, for some sub-DLAs, ionization corrections appear to be non-negligible (e.g. Richter et al. 2005; Quast et al. 2008).

1.1 This work: methodology and context

In this paper we present the case of a low column density sub-DLA towards the QSO J2123–0050 at $z_{\text{abs}} = 2.06$ whose unusual properties led us to re-assess the issue of ionization corrections for sub-DLAs. Since the methodology of this work differs from previous studies of ionization corrections in sub-DLAs, it is useful to summarise our approach at the outset. The superb data quality, in terms of both resolution ($R \sim 100,000$) and S/N (up to 50 per pixel), has permitted a rare chance to demonstrate the presence of a multi-phase medium, with contributions from both a mostly neutral component, and a more highly ionized component. Although many works on sub-DLAs have previously investigated ionization corrections in sub-DLAs (see above references), these investigations have uniformly assumed that the gas measured in absorption originates from a single phase. Since the sightline towards J2123–0050 firmly establishes that this is not always the case, our main objective is to answer the following question: ‘If multi-phase media are common in (sub)-DLAs, what will be the effect of calculating Cloudy ionization corrections with only a single phase?’.

In order to address this question we create a range of models with two-phase media, in which we vary the fractions of the ‘cold’ and ‘warm’ gas (as characterised by different ionization parameters). These models yield column densities of species such as SiII, FeII, AlII and AlIII. The key to our model philosophy is that we take these column densities as ‘observed’ values and adopt the usual empirical strategies of observers, and the assumption that the medium is a single phase, to attempt to derive the input parameters. In essence, we are attempting to recover the input model, but using an incorrect assumption about the ionization structure. Ultimately, we will quantify how wrong the derived elemental abundances will be under the assumption of a single phase ISM. The utility of this approach is that the relative contributions of components of real multi-phase absorbers can rarely be constrained. Multi-phase models are therefore not usually possible in practice. Our models therefore provide an indication of the likely error associated with the (necessary) single-phase approach. Additional uncertainties, such as those associated with geometry or in the atomic data, are not considered in this investigation.

The paper is laid out as follows. In Section 2 we describe the observations and data reduction of the QSO J2123–0050 and describe the measurement of the $N(\text{H I})$ and metal species column densities. In Section 3 we discuss the puzzling nature of this sub-DLA in the context of its ISM properties, if no ionization corrections are applied. The general fidelity of single phase models in the multi-phase case is quantified in Section 5 and evidence for a multi-phase medium in J2123–0050 discussed in Section 4. Returning

to the specific case of J2123–0050, photoionization corrections are calculated and applied in Section 6. Results are summarised in Section 7. The molecular content (H_2 and HD) of this absorber are investigated in 2 companion papers (Malec et al. 2010; Tumlinson et al. in preparation).

2 OBSERVATIONS AND DATA REDUCTION

The sub-DLA towards J2123–0050 was observed with the High Resolution Echelle Spectrograph (HIRES) as part of a program to follow-up metal-strong absorbers identified in the Sloan Digital Sky Survey (SDSS) by Herbert-Fort et al. (2006). These absorbers are selected in an automated fashion which searches for absorption in 14 prominent resonance lines. From the ~ 20000 quasars searched, more than 2000 metal absorption systems have been identified. In $> 95\%$ of cases where $\text{Ly}\alpha$ is covered in the SDSS spectrum, the H I column density is found to be large and the absorber would be classed as a DLA (Kaplan et al. 2010). Follow-up of a sub-sample of these metal-line selected DLAs with HIRES has shown that the metallicity of these DLAs is approaching the solar value, even at $z \sim 2$ (Kaplan et al. 2010). The main results of our high resolution survey will be presented elsewhere. In this paper, we focus on the case of the $z_{\text{abs}} \sim 2.06$ absorber towards J2123–0050 ($z_{\text{em}} = 2.26$, $r = 16.44$).

A preliminary HIRES exposure of 2×2700 seconds of J2123–0050 with the C1 decker (equivalent to a 0.86 arcsec wide slit) obtained on August 18th 2006, revealed the detection of H_2 and fine structure lines of carbon at $z = 2.05930$. Given the good observing conditions and the brightness of the QSO, further HIRES observations were obtained on April 19 2006 with a total exposure time of 10,800 s but with the E1 decker (0.4 arcsec wide), which yields a resolution of $R \sim 100,000$ ($\text{FWHM} \sim 3 \text{ km s}^{-1}$). Such high resolution is beneficial when studying the coldest phases of the ISM, allowing us to potentially resolve even very narrow components of the diffuse gas (e.g. Narayanan et al. 2006). All observations were conducted with the blue cross disperser, an echelle angle of 0° , and cross-disperser angle of 1.0275° , yielding a total wavelength coverage of approximately 3000 – 6000 Å. For calibration purposes, a set of standard trace flats were obtained, as well as the spectra of ThAr lamps (arcs) using the same instrument settings. We also obtained a set of pixel flats (lamp flats) at the beginning of the observing run to determine the pixel-to-pixel variation across the detectors.

The data were reduced using the HIReDux routine which is a part of the XIDL package². The reduction involved the following procedures:

- (i) A flat field frame was produced from a stack of approximately 30 flat field exposures for each of the detector’s chips.
- (ii) In a similar manner, a combined trace flat frame is produced as a median over the series of standard flat images taken during the observing night. This frame is then used to define (trace) the echelle order boundaries (and find the order of curvature), and to determine the slit profile, which is used to correct the illumination pattern of the science frames.
- (iii) A wavelength solution is derived from the spectra of a ThAr lamp taken with the same setup as in the science frames. HIReDux performs a 1D wavelength solution by fitting a low-order Legendre polynomial to the pixel values in the ThAr exposures versus the

¹ Different naming conventions have emerged for absorbers that exhibit damping wings, yet do not qualify as DLAs. The most common alternative name is super-Lyman limit system, e.g. O’Meara et al. (2007).

² XIDL is publicly available at <http://www.ucoick.org/~xavier/IDL/index.html>

laboratory wavelengths along the spatial centres of each order. The code then performs a 2D fit to all the lines from the 1D solution. Finally, the pipeline derives the 2D wavelength map giving both the wavelength solution, and the line tilts for all orders over the full echelle footprint.

(iv) After the raw science frame images are flattened and cosmic rays are flagged, the final step in the reduction process is the extraction of the object and the sky spectra. The sky background is estimated from the pixels that fall well beyond the object aperture, taking into account diffuse scattered light, which is estimated by interpolating the pixel counts in the gaps between the pixel orders. After this, the procedure derives the spatial profile of the object point spread function, and performs an optimal extraction based on the order trace.

(v) The individual exposures were coadded by combining each order separately, yielding a final, unnormalized 2D spectrum.

(vi) The continuum is fitted manually using the XIDL routine *x_continuum*. The routine allows the user to select the parts of the continuum unaffected by absorption and then performs a minimum χ^2 fit on the selected data points using a spline function of a given order (for the HIRES data presented here the usual value of the spline order is around 8).

(vii) The echelle orders are combined after normalization into a 1D spectrum. In regions of order overlap, the orders are averaged, weighting by the square of median signal-to-noise ratio. The final spectrum has a S/N of ~ 15 per pixel at 3100 Å, ~ 30 at 3500 Å, and ~ 40 at 5100 Å.

2.1 $N(\text{H I})$ determination

To perform the column density measurement of the Ly α absorption, the continuum and the line profile were simultaneously fit in a blaze-corrected section of the spectrum. The fit was performed using the *x_fitdla* routine of XIDL. The Ly α profile is clearly asymmetric, with the red wing showing stronger damping. The asymmetry indicated that a two-component fit was necessary. The redshifts of the components were fixed at the redshifts of the strongest metal line absorption in the two kinematically distinct metal line complexes detected in the system (see the next Section). The fit is presented in Figure 1. The column densities of the separate components are $\log N(\text{H I } z = 2.05930) = 19.18 \pm 0.15 \text{ cm}^{-2}$, and $\log N(\text{H I } z = 2.05684) = 18.40 \pm 0.30 \text{ cm}^{-2}$, yielding a total column density of neutral hydrogen of $\log N(\text{H I}) = 19.25 \pm 0.2 \text{ cm}^{-2}$. Note that these uncertainties are dominated by systematic (e.g. continuum fitting), not statistical error.

2.2 Metal column density measurements

In order to derive the total column density of multi-component metal line complexes VPFIT 9.3³ was used on the normalized data. VPFIT is a multiple Voigt profile fitting code that calculates a maximum likelihood fitting function to the data. The code is adapted to fit multiple lines simultaneously, which allows for efficient identification of blends. The goodness of fit is assessed in VPFIT by χ^2 statistics. The error estimates of the fitting parameters also include the uncertainties induced by self-blends, as well as blends due to unidentified lines. The errors on individual components are fairly poorly constrained, but the total column density error can be more accurately quantified and may be quite small, especially

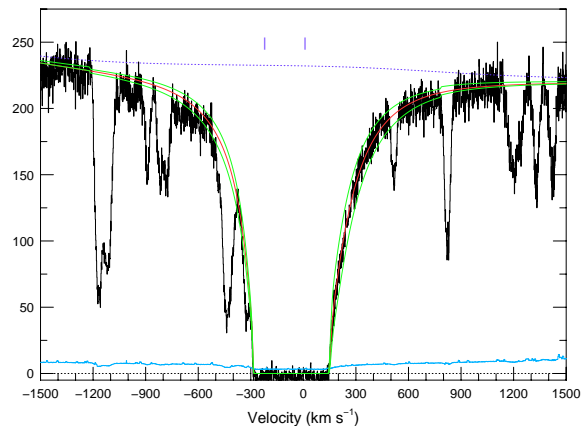


Figure 1. Fit to the Ly α line with total $\log N(\text{H I}) = 19.25 \pm 0.2 \text{ cm}^{-2}$ (red line). The blue dotted line represents the continuum fit and green lines are the 3σ bounds respectively. A two component fit (shown by tick marks) is required to adequately fit the asymmetric profile. The column densities of separate components are $\log N(\text{H I } z = 2.05930) = 19.18 \pm 0.15 \text{ cm}^{-2}$, and $\log N(\text{H I } z = 2.05684) = 18.40 \pm 0.30 \text{ cm}^{-2}$. The lower solid (cyan) line shows the 1σ error array.

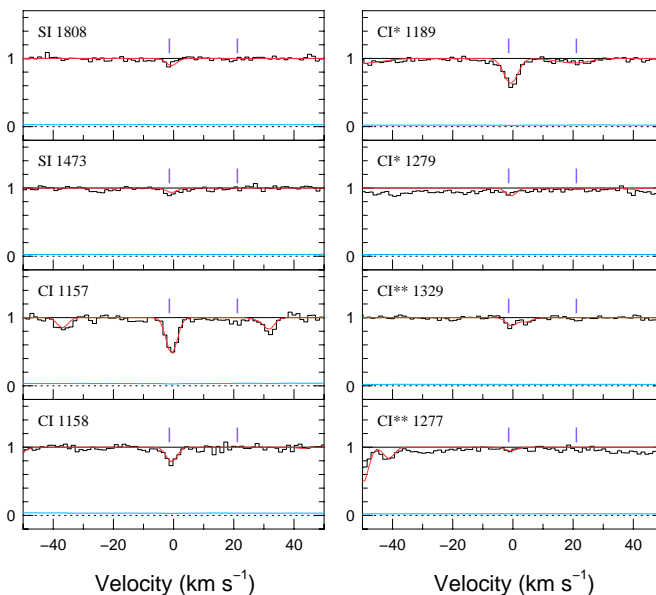


Figure 2. Fit to neutral carbon and sulphur lines towards J2123–0050 on a velocity scale relative to $z = 2.05930$. The ticks mark the position of the velocity components which give rise to molecular absorption. The data is presented in black, the error array is given in blue, and the fit is the red line.

³ www.ast.cam.ac.uk/~rfc/vpfit.html

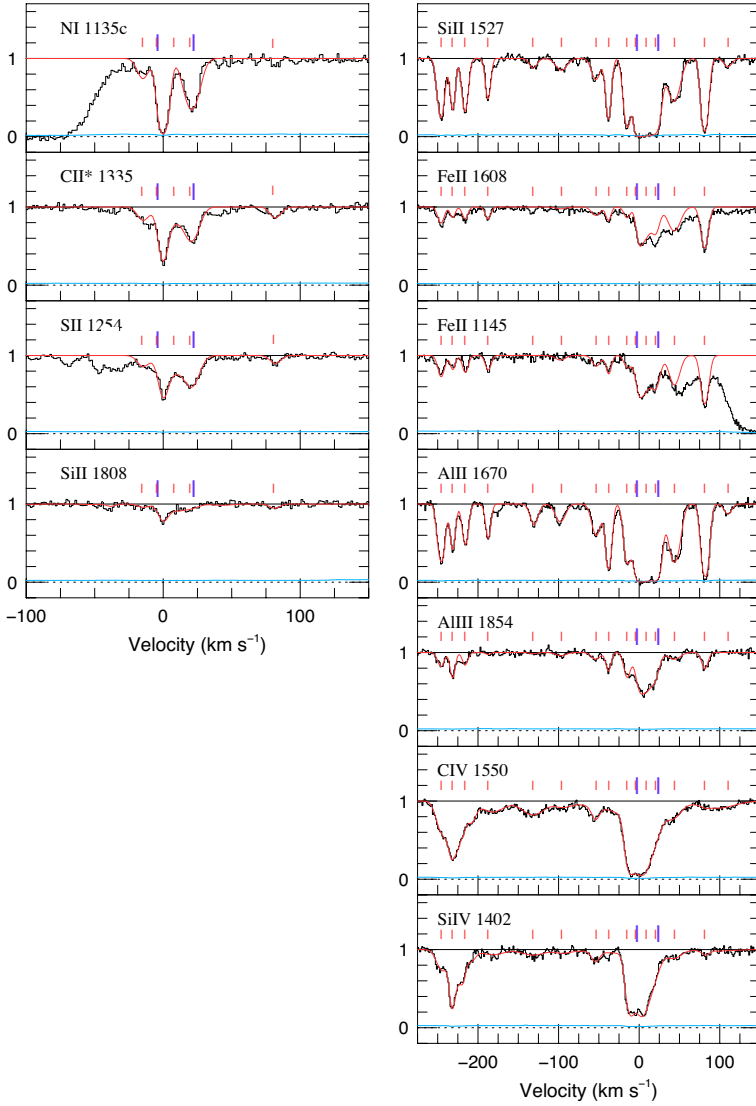


Figure 3. Metal lines towards J2123–0050 on a velocity scale relative to $z = 2.05930$. The long blue ticks mark the position of the velocity components which give rise to molecular absorption. The short red tick marks indicate other fitted components. The data is presented in black, the error array is given in blue, and the fit is the red line.

if several species are fit simultaneously with the same structural model. Lower limits are reported for species with only saturated transitions and 3σ upper limits are quoted for non-detections using the following equations:

$$W_{obs(3\sigma)} = 3 \times FWHM/(S/N), \quad (1)$$

$$W_r = W_{obs}/(1+z), \quad (2)$$

$$N = 1.13e20 \times W_r/(\lambda_r^2 \times f), \quad (3)$$

where W_r , and λ_r are rest-frame equivalent width and wavelength, f is oscillator strength, and (S/N) is signal to noise ratio at the observed line wavelength. Eqn 3 comes from the linear part of the curve of growth (e.g. Pagel 1997).

Table 1. Neutral carbon and silicon column densities from Voigt profile fits.

z	b (km s^{-1})	$\log N(\text{CI})$ (cm^{-2})	$\log N(\text{CI}^*)$ (cm^{-2})	$\log N(\text{CI}^{**})$ (cm^{-2})	$\log N(\text{SI})$ (cm^{-2})
2.05930	1.8 ± 0.3	13.73 ± 0.02	13.42 ± 0.03	12.43 ± 0.02	12.08 ± 0.05
2.05955	7.3 ± 4.0	12.91 ± 0.03	12.74 ± 0.10	12.16 ± 0.11	...
Total		13.79 ± 0.02	13.50 ± 0.03	12.62 ± 0.03	12.08 ± 0.05

z	b (km s ⁻¹)	log N(SiII) (cm ⁻²)	log N(FeII) (cm ⁻²)	log N(NiII) (cm ⁻²)	log N(AlII) (cm ⁻²)	log N(AlIII) (cm ⁻²)	log N(SII) (cm ⁻²)	log N(NI) (cm ⁻²)	log N(CII) (cm ⁻²)	log N(CII*) (cm ⁻²)
2.05684	5.2 ± 0.2	13.43 ± 0.02	12.93 ± 0.06	11.86 ± 0.04
2.05698	3.9 ± 0.2	13.20 ± 0.02	12.62 ± 0.09	12.05 ± 0.03
2.05714	4.5 ± 0.2	13.28 ± 0.02	12.72 ± 0.08	11.74 ± 0.05
2.05743	3.9 ± 0.3	13.03 ± 0.02	12.74 ± 0.07	10.85 ± 0.37
2.05800	6.2 ± 1.5	12.46 ± 0.08	10.81 ± 0.44
2.05836	8.5 ± 1.3	12.71 ± 0.05	12.14 ± 0.32	11.39 ± 0.14
2.05880	7.3 ± 0.8	12.90 ± 0.04	12.75 ± 0.08	11.65 ± 0.07
2.05896	4.0 ± 0.2	13.35 ± 0.02	12.74 ± 0.06	11.89 ± 0.04
2.05919	5.2 ± 0.2	13.57 ± 0.03	12.74 ± 0.05	12.13 ± 0.03	13.72 ± 0.06	13.38 ± 0.04	...	12.55 ± 0.07
2.05930	4.8 ± 0.1	14.18 ± 0.06	13.18 ± 0.07	11.86 ± 0.07	14.16 ± 0.04	14.34 ± 0.02	...	13.35 ± 0.03
2.05943	11.3 ± 0.9	14.11 ± 0.06	13.43 ± 0.07	12.73 ± 0.02	14.07 ± 0.07	12.78 ± 0.16
2.05955	6.4 ± 0.2	13.82 ± 0.05	13.24 ± 0.05	12.06 ± 0.04	14.20 ± 0.03	14.00 ± 0.02	...	13.19 ± 0.03
2.05979	10.1 ± 0.5	13.45 ± 0.02	13.40 ± 0.04	11.79 ± 0.06	12.62 ± 0.06
2.06017	5.0 ± 0.2	13.68 ± 0.02	13.49 ± 0.02	11.92 ± 0.04	13.43 ± 0.10
2.06047	6.5 ± 2.0	12.40 ± 0.11
Total		14.69±0.02	14.12±0.02	≤ 11.66	≥ 13.51	13.06 ± 0.04	14.70±0.02	14.53±0.02	≥ 15.2	13.71±0.01

Table 2. Metal ions column densities from Voigt profile fits. The upper section (separated by double horizontal lines) shows fits for the satellite complex, the lower section for the main complex, as defined in the text. Totals in the bottom row are only for the main complex (lower section)

Table 3. CIV and SiIV column densities from Voigt profile fits. The upper table section shows fits for the satellite complex, the lower section for the main complex, as defined in the text. The totals in the bottom row also refer only to the main complex.

z	b (km s ⁻¹)	log N(CIV) (cm ⁻²)	log N(SiIV) (cm ⁻²)
2.05685	9.0 ± 0.5	13.32 ± 0.08	12.70 ± 0.07
2.05695	6.6 ± 3.2	13.21 ± 0.73	12.07 ± 1.05
2.05698	4.1 ± 0.4	13.18 ± 0.45	13.00 ± 0.09
2.05704	4.0 ± 1.2	13.15 ± 0.32	12.47 ± 0.30
2.05711	4.7 ± 0.9	13.05 ± 0.15	12.68 ± 0.11
2.05721	7.5 ± 0.9	13.04 ± 0.06	12.34 ± 0.07
2.05749	19.5 ± 1.6	13.12 ± 0.03	12.39 ± 0.04
2.05800	18.7 ± 1.0	13.21 ± 0.02	12.40 ± 0.03
2.05838	13.5 ± 2.2	12.60 ± 0.11	12.01 ± 0.10
2.05879	6.3 ± 0.4	12.75 ± 0.03	12.22 ± 0.04
2.05916	55.4 ± 11.8	13.48 ± 0.17	12.68 ± 0.14
2.05923	6.6 ± 0.2	13.83 ± 0.05	13.30 ± 0.04
2.05930	8.8 ± 1.2	13.96 ± 0.18	13.38 ± 0.23
2.05943	28.6 ± 7.4	13.50 ± 0.10	12.88 ± 0.13
2.05947	12.8 ± 3.8	13.68 ± 0.34	13.23 ± 0.32
2.05978	12.1 ± 1.9	12.95 ± 0.16	12.37 ± 0.12
2.06018	6.3 ± 1.2	11.78 ± 0.29	11.83 ± 0.07
2.06033	28.4 ± 3.2	13.08 ± 0.07	11.96 ± 0.13
Total		14.48 ± 0.01	13.86 ± 0.01

The same kinematic structure (i.e. combination of Doppler (b) parameter and z) was used for singly ionized species, N I and Al III, but this model was not applicable to the more highly ionized species of C IV and Si IV. We also adopted an independent model for S I and C I, since these atoms likely trace gas in a cooler kinematic phase. The fits for the measured species are given in Tables 1 to 3 and shown in Figures 2 and 3.

2.3 Molecular hydrogen

Molecular transitions of hydrogen from both Lyman and Werner bands up to rotational level $J = 5$ are detected in two kinematically distinct components, at the velocity of the strongest metal complex. The H₂ lines are located at the same redshifts as the neutral lines of carbon, which are also aligned with the strongest singly ionized metal ion lines. Fitting the H₂ absorption features is complicated by saturation of the lowest J states and by the need for continuum and zero-level adjustment. Molecular HD is also detected in this system, only the third such detection in a DLA (see also Varshalovich et al 2001; Srianand et al. 2008). The HD and H₂ lines are analysed in two separate papers (Malec et al. 2010; Tumlinson et al. in preparation). The molecular lines are not considered further in this paper, but their presence is noted here for completeness.

3 CHEMICAL ABUNDANCES, MOLECULAR FRACTION AND COOLING RATE

The abundances, calculated on the basis of the raw column density measurements (uncorrected for ionization), in the sub-DLA towards J2123–0050 reveal a number of surprising results. These values, calculated relative to the solar abundance pattern of Grevesse, Asplund, & Sauval (2007), are given in Table 4. We consider only

Table 4. Elemental abundances before ($[X/H]_{raw}$) and after ($[X/H]_{corr}$) ionization corrections (IC(X/H)). Values are for the main complex whose $N(H\text{I})=19.18\pm 0.15$ cm⁻². Errors in $[X/H]$ account for the error in $N(H\text{I})$ and $N(X)$ and are added in quadrature. For presentation purposes, the errors are only quoted for the final corrected abundance, but the errors on the raw abundance are identical.

	log N(SiII) (cm ⁻²)	log N(FeII) (cm ⁻²)	log N(SII) (cm ⁻²)	log N(NI) (cm ⁻²)
Total	14.69±0.02	14.12±0.02	14.70±0.02	14.53±0.02
log(X/H) _⊙	-4.49	-4.55	-4.84	-4.22
[X/H] _{raw}	+0.00	-0.51	+0.36	-0.43
IC(X/H)	+0.71	+0.26	+0.55	-0.04
[X/H] _{corr}	-0.71 ± 0.15	-0.77 ± 0.15	-0.19 ± 0.15	-0.39 ± 0.15

the main absorption complex in this analysis, using an $N(H\text{I}) = 19.18$.

3.1 Metallicity Without Ionization Corrections

Uncorrected for ionization, the metallicity of the sub-DLA (main complex) appears to be super-solar, i.e. $[Si/H] = +0.00$ and $[S/H] = +0.36$. Super-solar metallicities have previously been presented for a small number of sub-DLAs in the literature (e.g. Prochaska et al. 2006; Peroux et al. 2006; Peroux et al. 2008; Meiring et al. 2008; Dessauges-Zavadsky et al. 2009), based on a similar analysis (i.e. assuming small or negligible ionization corrections). Such high metallicities are somewhat surprising at high redshift for a number of reasons. First, the emission line abundances measured from actively star-forming galaxies at $z > 2$ are almost exclusively sub-solar (e.g. Erb et al. 2006; Maiolino et al. 2008). It is feasible that absorption and emission line abundances yield discrepant results (e.g. Ellison, Kewley & Mallen-Ornelas 2005) due to abundance gradients and/or local enrichment. However, although the magnitude of H II-to-H I region abundance disagreements is still debated (e.g. Leboutteiller et al. 2009 and references therein), it would be expected that any discrepancy would tend towards higher abundances for emission lines. Moreover, emission line abundances measure only the metallicities of the actively star-forming regions, whereas absorption line measurements probe the entire galaxy along a given sightline and therefore yield average ISM measurements. Even in cases where a sightline probes regions near active star-formation, such as the case for GRB-absorbers, metallicities are typically around 1/10 Z_{\odot} (Prochaska et al. 2007a).

3.2 Relative Abundances Without Ionization Corrections

Although the range of elements probed by our spectra is somewhat limited, there are two notable abundance ratios of interest. The first are indicators of α element enhancement, which can be obtained from the ratios of $[S/Fe] = +0.87$ and $[Si/Fe] = +0.51$. The complexities of interpreting such ratios in the context of nucleosynthetic versus dust effects have been discussed by many authors (e.g. the review by Wolfe et al. 2005). What is striking in the case of J2123–0050 is the extremely high values of $[S,Si/Fe]$ compared to previous measurements (e.g. Prochaska & Wolfe 2002).

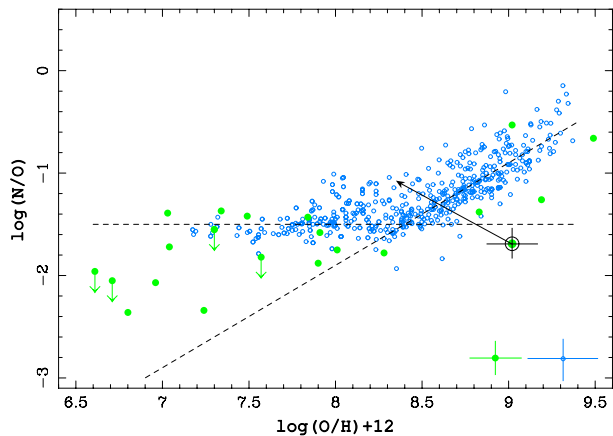


Figure 4. N/O ratio plotted against the system metallicity on the solar scale. Metallicities are determined from O/H or Si, S/H corrected by the solar ratio of Si/O or S/O (see Table 4). The sub-DLA towards J2123–0050 (ringed green circle) is plotted against the DLA data (green circles) and Galactic H II regions (open blue circles) assembled by Pettini et al. (2008). The dashed lines show predicted contributions from primary and secondary N production. The arrow points to the J2123–0050 ratio corrected for ionization. Representative error bars for H II regions and DLAs are given in the lower right of the figure.

The main complication here is the unquantified effect of dust depletion, particularly for Fe II which can raise these ratios far above their intrinsic values.

A second ratio which reveals a surprising result is N/S. The utility of nitrogen as a cosmic clock, thanks to its primary and secondary contributions, has been discussed extensively in the literature (e.g. Pettini et al. 2002, Prochaska et al. 2002a; Centurion et al. 2003; Henry & Prochaska 2007; Petitjean et al. 2008). In brief, the dominant contribution of α elements to the ISM comes from prompt enrichment by massive stars which result in Type II SN. Secondary nitrogen is released on a longer timescale, once the seed nuclei of carbon have been established from previous generations of stars. Hence, the secondary component of nitrogen steadily builds with time once the metallicity is approaching the solar value. The source of primary nitrogen is still a contentious issue, but the substantial scatter of N/α in DLAs has led to the suggestion that primary nitrogen production occurs in low or intermediate mass stars and its release is hence delayed relative to the α elements (Pettini et al. 2002; Henry & Prochaska 2007).

The sub-DLA towards J2123–0050 is the first QSO absorber with solar or super-solar metallicity in which N has been measured. At such high metallicities, Galactic H II regions show N/α ratios that are correlated with metallicity (usually measured from O/H) as expected from the secondary production mechanism described above. In Figure 4 we show the ratio of N/α in the J2123–0050 sub-DLA along with other DLA N measurements from the literature and Galactic H II regions. The sub-DLA lies in a previously unpopulated part of the diagram – high metallicity, but relatively low N/α . This is a puzzling result. On the one hand, this DLA has apparently experienced sufficient star formation to enrich its ISM to above solar values, but is only experiencing primary nitrogen enrichment. One explanation of this combination of abundances would be that the galaxy is both chemically young, but has experienced intense and productive star formation.

3.3 Cooling rate

The sub-DLA towards J2123–0050 is also an outlier in the cooling rate distribution of DLAs. Wolfe et al. (2003) derived a method to determine the properties of the star forming regions associated with the DLA sightlines through the detection of the C II* $\lambda 1335$ line. The method estimates [C II] $158\mu\text{m}$ emission from the strength of the C II* $\lambda 1335$ absorption. Absorption resulting in the 1335 \AA line arises from $^2P_{3/2}$, from which a $158\mu\text{m}$ photon is spontaneously emitted during the decay to the $^2P_{1/2}$ fine-structure state in the ground $2s^22p$ term of C II. The [C II] $158\mu\text{m}$ transition is a principal coolant of interstellar neutral gas in the Galaxy (Wright et al. 1991). By assuming that cooling is dominated by the $158\mu\text{m}$ line, the heating rate can be calculated by determining the [C II] cooling rate l_c .

The emissivity of [C II] $158\mu\text{m}$ can be calculated from the column density of C II* $\lambda 1335$ line following the expression of Potasch, Wesselius, & van Duinen (1979):

$$l_c = \frac{N(\text{CII}^*)hv_{ul}A_{ul}}{N(\text{HI})} \text{ ergs s}^{-1} \text{ Hz}^{-1} \quad (4)$$

where A_{ul} is the Einstein A coefficient, and hv_{ul} is the energy of the $158\mu\text{m}$ transition. For the sub-DLA towards J2123–0050, we derive $l_c = 1.03 \times 10^{-25} \text{ ergs s}^{-1} \text{ Hz}^{-1}$. Wolfe et al. (2008) have recently shown that l_c in DLAs follows a bimodal distribution with a transition at $l_c \sim 10^{-27} \text{ ergs s}^{-1} \text{ Hz}^{-1}$. Absorbers above this critical value exhibit higher metallicities, velocity widths and dust-to-gas ratios. Furthermore, Wolfe et al. (2008) suggest that galaxies with cooling rates higher than the critical value are located in more massive halos with active star formation occurring in ‘bulge mode’, i.e. removed from the gas halo. Although the sub-DLAs towards J2123–0050 qualitatively follows the above trend with its super-solar metallicity and complex velocity structure, it has a cooling rate that exceeds all the values in the Wolfe et al. (2008) DLA sample by a factor of ten (although saturation of the C II leads to lower limits for l_c , especially at high $N(\text{HI})$), and is also larger than the average Galactic disk value.

4 EVIDENCE FOR A MULTI-PHASE MEDIUM

The neutral inter-stellar medium is generally divided into two components – a warm neutral medium (WNM) with temperatures of several thousand degrees K and densities $\sim 0.1 \text{ atoms cm}^{-3}$, and the cold neutral medium (CNM) with $T \sim 100 \text{ K}$ and $n \sim 10 \text{ atoms cm}^{-3}$ (Field et al. 1969). Spin temperatures of high redshift DLAs are generally high (e.g. Kanekar et al. 2006 and references therein), with only one DLA exhibiting a value below 350 K at $z_{\text{abs}} > 1$ (York et al. 2007). These high values are consistent with sightlines that intersect both CNM and WNM gas. Kanekar, Ghosh & Chengalur (2001) show this temperature segregation explicitly for one DLA at $z_{\text{abs}} \sim 0.2$. At higher redshift, absorption from a range of high and low ionization species indicates that a multi-phase structure in DLAs is common (e.g. Wolfe & Prochaska 2000; Fox et al. 2007; Lehner et al. 2008; Quast et al. 2008). In this section, we examine the evidence for a multi-phase medium in the sub-DLA towards J2123–0050.

The sub-DLA towards J2123–0050 is a kinematically complex system with metal absorption spreading over 400 km s^{-1} in velocity space requiring 15 components for a reasonable Voigt profile fit, see Figure 3. Although such a wide velocity spread is not unique amongst quasar absorbers, this sub-DLA is unusual in the range of species that are detected. In addition to the often-observed

singly ionized species, such as Si II and Fe II, the much less common C I line is present and a rare detection of S I (see also Quast et al. 2008). Substantial column densities of more highly ionized species are also measured, for example, for Al III, C IV and Si IV. The singly and multiply ionized metal species are clearly separated into a main complex centred at $z_{\text{abs}} = 2.05934$ and a satellite complex at $z_{\text{abs}} = 2.05684$ (i.e. separated by $\sim 250 \text{ km s}^{-1}$). The neutral species, such as C I and S I are detected in only two components of the main complex. The same is true for the molecular absorption (Malec et al. 2010; Tumlinson et al. in prep) which is observed in only one (HD) or two (H₂) velocity components associated with the main complex. The simultaneous presence of such a variety of ionized species for a given element and the kinematic diversity is strongly suggestive of a multi-phase medium in which neutral and molecular species occupy only a fraction of the interstellar volume.

Further evidence for a multi-phase medium comes from the details of the Voigt profile fit. The neutral carbon and sulphur lines require a very small b -parameter of only 1.8 km s^{-1} . These very narrow lines are unresolved even in this high resolution spectra ($R \sim 100,000$). However, because of a high range of gf values in which C I transitions are observed, the b -parameters of these lines are constrained well. The singly ionized species are more than twice as broad with b -parameters $\sim 4.8 \text{ km s}^{-1}$, such differences are common signatures in the Galactic ISM (e.g. Spitzer & Jenkins 1975). Ignoring the contribution of turbulence in line broadening, for a given chemical element that is detected in multiple ionization stages, the ratio of Doppler parameters scales as the square root of the ratio of temperatures, a factor of seven in the case of neutral and singly ionized sulphur. The sub-DLA studied here therefore presents a clear case of a multi-phase medium at high redshift.

5 IONIZATION MODELS FOR A TWO-PHASE MEDIUM

As discussed in the Introduction, ionization corrections are usually assumed to be negligible for DLAs, and have also been reported to be < 0.2 dex in sub-DLAs. Although this value is not large, corrections of this magnitude may be sufficient to mask nucleosynthetic signatures (e.g. Prochaska et al. 2002a; Quast et al. 2008). Previous attempts to model ionization corrections have assumed a single phase model. Our observations of J2123–0050 clearly demonstrate that this is not always an accurate assumption. However, single phase models are useful because they do not require knowledge of how much of the observed $N(\text{H I})$ is associated with each phase. As discussed by Ellison et al. (2007), it is extremely difficult to separate DLA Ly α profiles into separate components⁴, although species such as O I may provide clues in this respect (e.g. Fox et al. 2007). To assess the impact of the single-phase assumption we use Cloudy (Ferland et al. 1998) to construct a multi-phase model and then test how accurately the column densities can be recovered under the single-phase assumption.

The modelling procedure is as follows.

(i) A model with two phases is constructed, where the ‘phase’ is defined by the ionization parameter, i.e., the ratio of H ionizing photons to H atoms. The ‘cold’ phase gas is defined as having an ionization parameter of $\log U = -5.0$, while the ‘warm’ phase is set to $\log U = -3.0$. The total combined neutral column density of the cloud in both phases is set to be $N(\text{H I}) = 10^{19.18} \text{ cm}^{-2}$. Nine

versions of the model were constructed with different fractions of the $N(\text{H I})$ in the warm and cold phases ranging from completely cold to completely warm gas (essentially these extrema are single-phase clouds).

(ii) The metallicity of the cloud is fixed at $[\text{M}/\text{H}] = -0.33$ in all models, with a solar abundance pattern as given in Cloudy version 07.02.

(iii) The two-phase cloud is radiated with a mix of the Haardt-Madau (H&M) extragalactic spectrum (Haardt & Madau 1996) and the average Galactic ISM spectrum of Black (1987), which primarily affects the ions with ionization potential lower than 1 Ryd, such as C I, and S I.

(iv) For each of the nine models (which sample different fractions of cold and warm gas), Cloudy outputs the column densities of Fe II, S II, Si II, Al II and Al III separately for the cold and warm phase. The column densities of a given species in the cold and warm phases are summed to give the column densities that would be observed in a real spectrum.

The procedure described above yields nine sets of column densities for two-phase models. The next step is to recover the metallicity of the theoretical input cloud by following the steps that an observer would execute in trying to model the cloud with a single phase. This requires adopting a metallicity and an indicator of $\log U$ and then running Cloudy over a parameter grid until the observed values are reproduced. All grids are calculated using a mix of the H&M and the average Galactic ISM spectrum stopping the calculations when the column density of neutral hydrogen reaches $N(\text{H I}) = 10^{19.18} \text{ cm}^{-2}$. The details of this stage in the modelling are:

(i) For the metallicity, we assume $[\text{M}/\text{H}] = [\text{Fe II}/\text{H I}]$ (where the column densities come from the Cloudy output). In order to test whether this approximation of metallicity introduces a significant error, we also repeat the experiment with the ‘true’ metallicity of $[\text{M}/\text{H}] = -0.33$ (in practice, this is unknown to the observer).

(ii) The ionization parameter of the single-phase model of each of the theoretical clouds is inferred from the column density ratio of Al II/Al III. This ratio is commonly used as an indicator of ionization in sub-DLAs and DLAs (Dessauges-Zavadsky et al. 2003; Prochaska et al. 2002b). One of the empirical motivations for using Al II/Al III is its correlation with neutral hydrogen column density (Vladilo et al. 2001, Dessauges-Zavadsky et al. 2002). Narayanan et al. (2008) speculated that this anti-correlation might extend also to the lower column density QALs, such as weak Mg II absorbers. However, other work has questioned the utility of Al II/Al III for constraining the ionization parameter (e.g. Howk & Sembach 1999), whose atomic data is additionally poorly known (e.g. Vladilo et al. 2001; Dessauges-Zavadsky 2003). However, since our methodology is to adopt standard observational strategies to quantify errors in derived properties, we follow the common practice of using Al II/Al III to constrain ionization parameter. Figure 5 presents the inferred value of $\log U$ for each of the nine theoretical two-phase clouds. The left-hand panels show the results of the models in which the metallicity is estimated from Fe II/H I, whereas the right-hand panels show the models using the correct metallicity. The left-hand panels are almost identical to those on the right, indicating that, for these models, using Fe II/H I as an estimate for metallicity is a good approximation. As expected, Al II/Al III increases monotonically with $\log U$. Perhaps more surprising is that this approach fairly faithfully recovers the ionization parameter of the warm phase even if its contribution to the total neutral hydrogen density is as small as 10%. The difference between the real and recovered $\log U$ for the warm phase is only on the order of 0.10 dex.

⁴ At lower column densities, asymmetries in the Ly α wing become more obvious and separation becomes easier

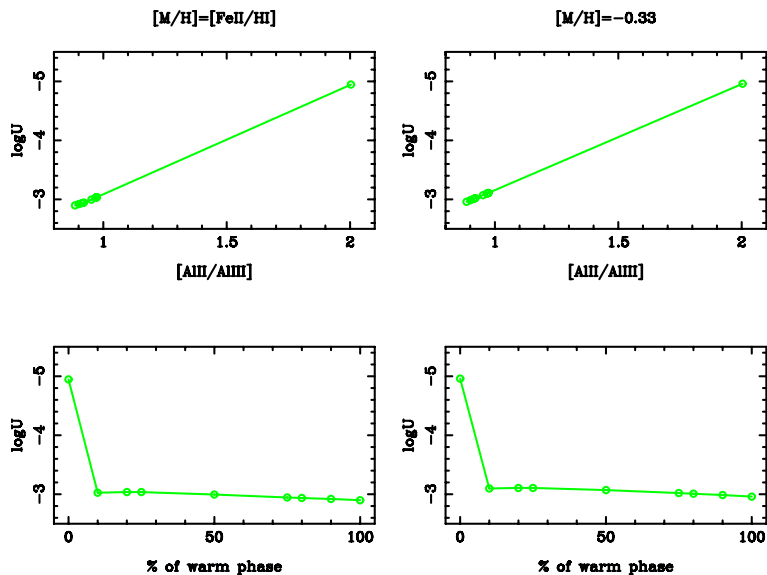


Figure 5. Derivation of the ionization parameter from aluminium ionic ratios calculated for theoretical two phase clouds, assuming a single phase. The top panels show a monotonic relation between $\text{Al II}/\text{Al III}$ and the inferred $\log U$. The lower panels show the inferred ionization parameter as a function of the fraction of N(H I) in the warm phase. The left hand column is for the single-phase models that assume $[\text{M}/\text{H}] = -0.33$, while the right is for models with $[\text{M}/\text{H}] = [\text{Fe II}/\text{H I}]$. Even if the contribution of the warm phase to the total column density of H I is as small as 10% the models recover the $\log U$ of the warm phase to within ~ 0.10 dex.

(iii) After the ionization parameter is derived for each model, the ionization corrections are calculated. The fractional column density of an element in a given ionization state is given as $f(\text{X}^{i+}) = \frac{N(\text{X}^{i+})}{N(\text{X})}$, and similarly for hydrogen $f(\text{H I}) = \frac{n(\text{H I})}{n(\text{H})} = \frac{N(\text{H I})}{N(\text{H})}$. The ionization corrections $IC(\text{X}/\text{H})$ are then given by:

$$IC(\text{X}/\text{H}) = \log\left(\frac{N(\text{X}^{i+})}{N(\text{H I})}\right) - \log\left(\frac{N(\text{X})}{N(\text{H})}\right), \quad (5)$$

which is simply:

$$IC(\text{X}/\text{H}) = \log\left(\frac{f(\text{X}^{i+})}{f(\text{H I})}\right), \quad (6)$$

These values are subtracted from the ionic abundances to obtain the final abundance of an element. Comparing these corrected abundances to the input values of the original two-phase model allows us to assess how accurately ionization corrections for a single phase model recover the input abundances of a truly two-phase medium.

The results of this experiment are presented in Figure 6 for the case where the intrinsic metallicity is known, and Figure 7, for the case which uses the ‘observed’ metallicity. The top panel presents the ‘observed’ ionic abundance for Si II , S II and Fe II , the middle panel shows the ionization corrections, and the bottom panel gives the corrected metallicities. The black line indicates the input metallicity of $[\text{M}/\text{H}] = -0.33$. Only the results for Si II , S II and Fe II are shown, as these are the ions measured in our study. For completeness, we also show in the Appendix a more complete set of models for a further six elements commonly measured in DLAs. The recovered metallicity for all of the two-phase models over-estimates the input value. However, the deviation from the $[\text{M}/\text{H}] = -0.33$ value is less than 0.15 dex for both metallicity models, with the error for Fe consistently lower than that of Si, and S. The accuracy

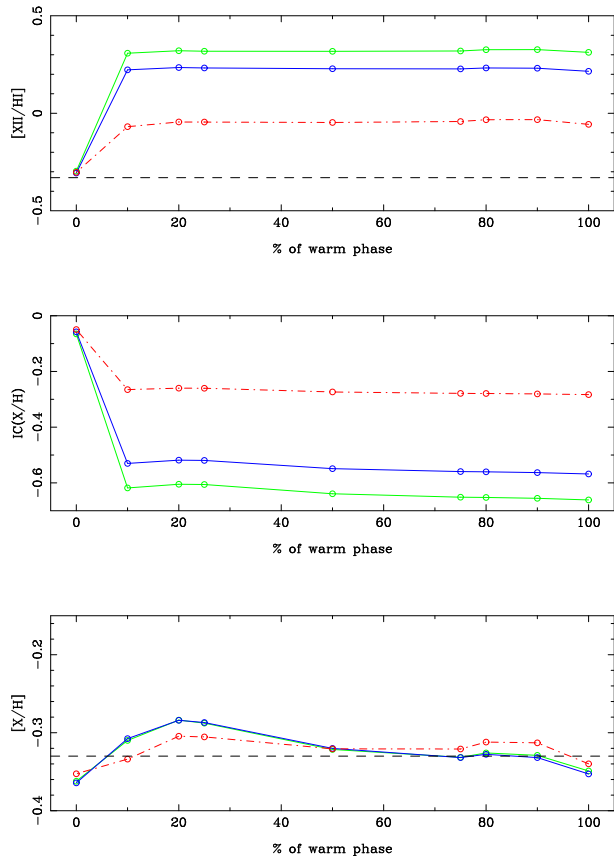


Figure 6. Ionization corrections for the theoretically modeled medium with $[\text{M}/\text{H}] = -0.33$. The ionic abundances ‘measured’ from the Cloudy models are presented in the top panel for Si II (green line), S II (blue line) and Fe II (red dotted line). The ionization corrections are given in the middle panel, and the corrected abundances are shown in the bottom panel. The black horizontal line represents the input metallicity of $[\text{M}/\text{H}] = -0.33$. The single-phase based corrections recover the metallicity of the clouds to within ~ 0.15 dex.

of the corrections increases with increasing warm-phase fraction. The input metallicity is recovered when the model is either 100% warm or 100% cold phase, since in these cases, the single-phase approximation is obviously an accurate one. From these models, it is possible to quantify the approximate accuracy to within which ionization corrections can be calculated from a single phase Cloudy model. The experiment also shows that if even a small fraction of hydrogen column density is present in the warm phase, applying no corrections to the elemental abundances can lead to over-estimates up to 0.5 dex (as is the case for Si in this example).

6 CORRECTED COLUMN DENSITIES FOR J2123–0050

In this section we derive photo-ionization corrections for the sub-DLA towards J2123–0050 based on a single-phase Cloudy model and present the corrected elemental abundances.

6.1 Cloudy model for J2123–0050

As shown in Section 5, for a multi-phase medium, the corrections derived from the single-phase Cloudy model approximate the values of the warm medium and become increasingly inaccurate as the

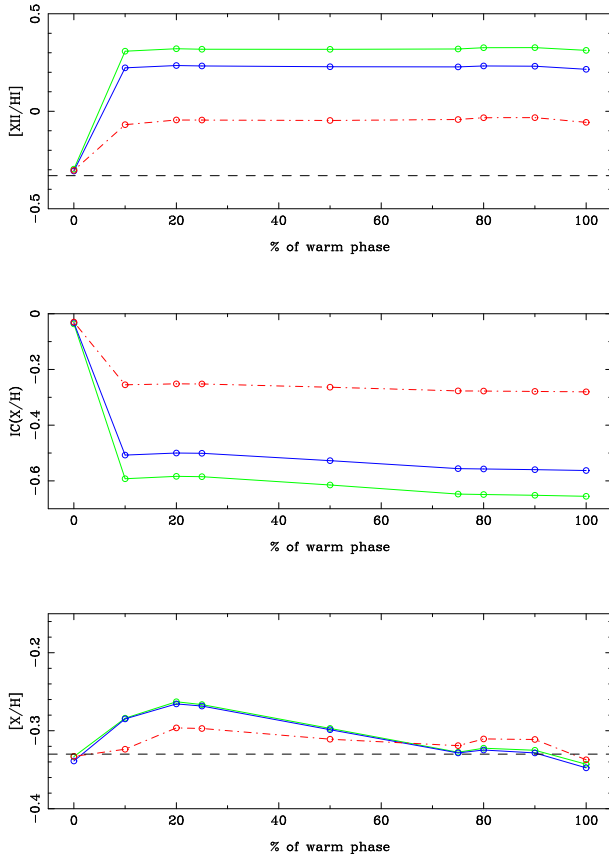


Figure 7. Same as in Figure 6, but for an assumed metallicity of $[M/H]=[Fe\ II/H\ I]$.

medium becomes dominated by a cooler phase. It is unfortunately not possible to model the corrections for J2123–0050 with a multi-phase medium since the distribution of neutral hydrogen between the phases is impossible to constrain. For the case simulated above, we have shown that although ionization corrections that assume a single phase medium may still tend to over-estimate the intrinsic abundances, this effect is typically at the <0.1 dex level. Applying no ionization correction can lead to abundance over-estimates of more than 0.5 dex. We therefore take the enforced approach of adopting a single-phase model, but with the knowledge that further corrections for the multi-phase structure are likely to be small. Additional sources of uncertainty present in the modelling of any given absorber with Cloudy include assumptions for the UV background, relative abundances, atomic data and absorber geometry.

To calculate the ionization corrections (eqn 6) for the sub-DLA J2123–0050 we constrain the Cloudy model to have $N(H\ I) = 10^{19.18}\text{ cm}^{-2}$, a metallicity of $+0.36$ (from the raw measurement of $S\ II$ and $H\ I$), and a solar abundance pattern. In order to determine the ionization parameter (which, as we have shown above, approximates to that of the warm medium if multiple phases are present), the code matches the observed $(Si\ II/Al\ III)$ ratio of 1.63 to the values obtained from the model (see top panel of Figure 8). $Si\ II$ is used as a proxy for $Al\ II$ since the only available $Al\ II$ line is saturated and only a lower limit to aluminium ionic ratio ($Al\ II/Al\ III > 0.45$) can be measured from the available spectrum.

The upper panel of Figure 8 presents the ionic ratio $(Si\ II/Al\ III)$ versus the ionization parameter from the model grid. The observed ratio of ions intercepts the model curve at the ionization parameter

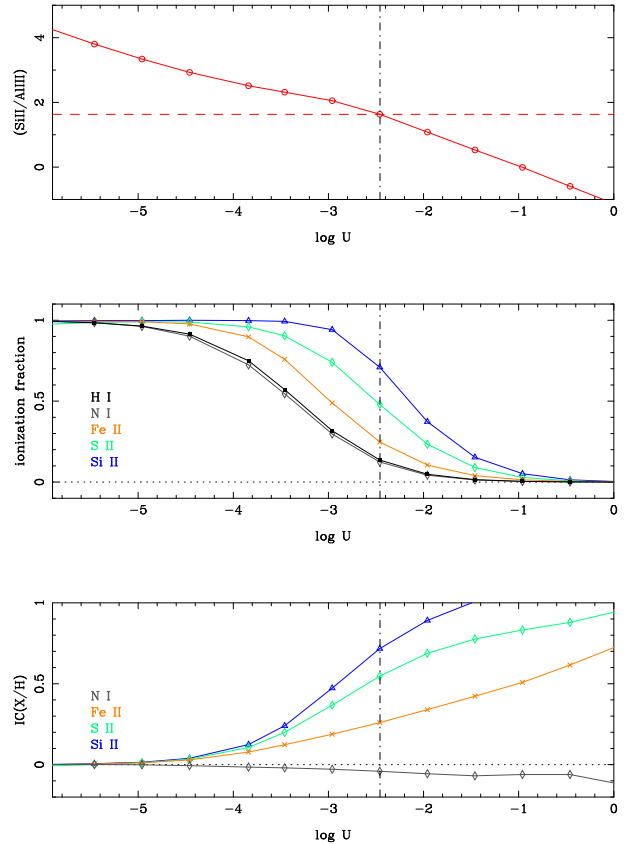


Figure 8. The top panel shows the predicted $Si\ II$ to $Al\ III$ column density ratio from the Cloudy models with the photoionizing spectrum containing both average Galactic ISM and extragalactic HM spectra. The horizontal dashed line is drawn at the measured ratio. The average ionization parameter inferred by comparing the observed values to the model has a value of -2.46 . The middle panel shows the fraction of each element in the given stage of ionization. Predicted ionization corrections for the selected metal abundances (see equation 6) from the same models are given in the lower panel.

of $\log U = -2.46$. The lower panels give the model inferred ionization fraction and correction curves for the ions of interest. Table 4 reports the ionization corrections (IC) for each element, and the corrected abundance on the solar scale once the ionization has been accounted for. The errors on the column densities are those determined by VPFIT (Table 2), and errors on abundances include the error in $N(H\ I)$ propagated in quadrature. No attempt has been made to estimate the error on the ionization correction due to the uncertainties mentioned above. Nitrogen (relative to $H\ I$) is the least affected by ionization, which is often implicitly assumed, due to its ionization potential of 1.07 Ryd. Indeed, the middle panel of Figure 8 shows that the fraction of $N\ I$ closely tracks the $H\ I$ as a function of $\log U$. $Si\ II$ is the species requiring the largest ionization correction for the limited species studied here (see the Appendix for corrections for other elements).

In order to examine the influence of the photoionizing spectrum and the assumed metallicity on the magnitude of the inferred corrections, additional Cloudy grids of varying metallicity (1/3 solar, and solar) and photoionizing radiation field (by scaling the Galactic ISM spectra component to 0, 1/10, 1/3, 3, and 10 of the original) were produced. The models with the combination of these parameters that acceptably reproduce the observed elemental abun-

dance ratios vary the magnitude of the resulting correction within a couple of tenths of a dex from the value determined by the original model.

6.2 Application of ionization corrections

We now re-examine the metallicity, cooling rate, N/α and α/Fe abundances of the sub-DLA towards J2123–0050 using ionization corrected metal abundances. Although the ‘raw’ abundances indicated that this sub-DLA had a super-solar abundance in both Si and S, the corrected abundances of all elements are below the solar value: $[\text{S}/\text{H}] = -0.19$ and $[\text{Si}/\text{H}] = -0.71$. This sub-DLA therefore remains metal-rich for its redshift, relative to DLAs at $z \sim 2$, superficially supporting the idea (e.g. Peroux et al. 2007) that sub-DLAs may be preferentially more metal-rich than DLAs. However, a recent re-appraisal of this hypothesis by Dessauges-Zavadsky et al. (2009) has argued that the difference in metallicity only exists at low redshift ($z_{\text{abs}} < 1.7$), and have suggested that this might be due to a selection effect. In the case of the sub-DLA towards J2123–0050, the comparison with the bulk of DLAs is not a fair one, since this system was selected to be metal-strong. Herbert-Fort et al. (2006) provided the first evidence that absorbers selected based on strong metal lines have a tendency to approach solar metallicity. This has been confirmed by Kaplan et al. (2010) who find typical metallicities of metal-strong DLAs at $z_{\text{abs}} \sim 2$ in the range of 1/10 to 1/3 of solar. The sub-DLA studied here is therefore consistent with the range of metallicities measured in identically selected, higher H I column density systems at the same redshift.

The determination of the cooling rate includes the $N(\text{H I})$ column density; for most Galactic interstellar sightlines the total hydrogen content is indeed dominated by neutral gas so that $N(\text{H I})$ is a reasonable proxy in the calculations (e.g. Pottasch et al. 1979). However, we have shown that this is not the case for the sub-DLA studied here. We therefore re-calculate the cooling rates as:

$$l_c = \frac{N(\text{C II}^*) h\nu_{ul} A_{ul}}{N(\text{H})} \text{ erg s}^{-1} \text{ Hz}^{-1} \quad (7)$$

where the total hydrogen column density determined from our ionization model is $\log N(\text{H}) = 20.05 \text{ cm}^{-2}$. The cooling rate calculated for J2123–0050 decreases from $l_c = 1.03 \times 10^{-25} \text{ ergs s}^{-1} \text{ Hz}^{-1}$ to $l_c = 1.39 \times 10^{-26} \text{ ergs s}^{-1} \text{ Hz}^{-1}$, consistent with the ‘high-cool’ population studied by Wolfe et al. (2008).

Finally, the corrected N/O ratio has also moved dramatically relative to its ‘raw’ values, due to both corrections in metallicity and N/O (determined from N/S with a correction for the S/O solar abundance). The corrected value (see Figure 4) is now indicative of a primary plus secondary nitrogen contribution and is consistent with Galactic H II regions at a similar metallicity. Concern regarding ionization corrections of N/α ratios has been previously raised, e.g. Izotov et al. (2001). Specifically, ionization effects have been appealed to in order to explain the large scatter of N/α ratios below the primary plateau. Although we have shown that a significant correction is required for the sub-DLA studied here, Pettini et al. (2002) have argued that such corrections are unlikely to be responsible for all of the observed scatter.

7 SUMMARY AND DISCUSSION

The ISM is expected to exhibit a multi-phase structure and there is abundant evidence that DLAs are no exception. In this paper we

present the case of a $z_{\text{abs}} = 2.06$ sub-DLA which exhibits a complex kinematic and ionization structure. The HIRES data obtained represent one of the highest resolution spectra obtained of a high z QSO which facilitates the study of the multi-phase ISM. Absorption transitions detected in this sub-DLA range from species which trace cold gas (such as H₂, HD, S I, C I) up to highly ionized species such as C IV. Ignoring ionization corrections in this system leads to puzzling properties.

We have shown that using a single phase model to derive ionization corrections in a multi-phase medium can only recover abundances to within ~ 0.15 dex (for the model example investigated here). Although the exact accuracy of corrections will depend on a large number of factors (input ionizing spectrum, number of phases, their ionization parameters etc.), our experiment illustrates that caution is required when interpreting abundances in sub-DLAs. For coarse properties, e.g. distinguishing a solar metallicity galaxy from one a metal-poor one with $Z \sim 1/10 Z_{\odot}$, the single-phase assumption probably does not impact greatly on the conclusions. However, relative abundances, which are used to identify subtle nucleosynthetic effects, may be quite susceptible to ionization errors. For example, although our two-phase model was constructed with a solar ratio of Si/Fe, the output abundances (see Figures 6 and 7) yielded an over-abundance of Si by up to 0.1 dex. This might otherwise be interpreted as evidence for dust depletion in Fe, or α -element enhancement in Si.

In closing, we note that the sub-DLA studied here is of particularly low $N(\text{H I})$, and is unusual in the range of ionization species it displays. It may therefore not be typical of the sub-DLA population as a whole. However, it does alert us to the real need to assess the ionization state of sub-DLAs on a case by case basis. For example, Quast et al. (2008) recently revisited the $z_{\text{abs}} = 1.15$ absorber towards HE0515–44. Originally estimated by de la Varga et al. (2000) to have $\log N(\text{H I}) \approx 20.45$, Hubble Space Telescope spectra yield $\log N(\text{H I}) = 19.9 \text{ cm}^{-2}$ (Reimers et al. 2003). As for the sub-DLA studied here, Quast et al. (2008) detect a range of ionization species including S I, Si I, Fe I, Si III and Al III which confirm that the sightline intersects a combination of neutral and ionized gas. In fact, Quast et al. (2008) conclude that the majority of the metal line species in the sub-DLA towards HE0515–44, similarly to the one in J2123–0050, are formed in the ionized component. A second interesting example is the absorber at $z_{\text{abs}} = 0.745$ towards Q1331+17. Ellison et al. (2003) previously investigated the complex kinematic structure and ionization structure of this absorber. A HIRES spectrum obtained by one of us (JXP) also exhibits Si I and Fe I, ions also reported by D’Odorico (2007), although neither of these cases has coverage of higher ionization species. The $N(\text{H I})$ of the $z_{\text{abs}} = 0.745$ absorber towards Q1331+17 is not known, but its D -index (Ellison 2006; Ellison et al. 2008) indicates that it is likely to be a sub-DLA. There are thus three cases where sub-DLAs exhibit absorption from neutral gas, presumably a cold phase, despite their relatively low $N(\text{H I})$. In at least two of these cases, higher ionization species are also present, a strong indication that the sightline is intersecting multi-phase gas. Although it is difficult to draw robust conclusions from such small numbers, one explanation could be that the $N(\text{H I})$ column density of *some* sub-DLAs is low because of ionization from H I to H II, as well as a conversion of H I to H₂ (e.g. Schaye et al. 2001; Krumholz et al. 2009). Although Noterdaeme et al. (2008) do not find a strong correlation between $N(\text{H I})$ and the probability of H₂ detection, the sample of the sub-DLA population is relatively sparse. A more extensive survey of neutral ions such as C I in DLAs and sub-DLAs would be most interesting in this regard.

ACKNOWLEDGMENTS

SLE is supported by an NSERC Discovery Grant. The data presented herein were obtained at the W.M. Keck Observatory, which is operated as a scientific partnership among the California Institute of Technology, the University of California and the National Aeronautics and Space Administration. The Observatory was made possible by the generous financial support of the W.M. Keck Foundation. The authors wish to recognize and acknowledge the very significant cultural role and reverence that the summit of Mauna Kea has always had within the indigenous Hawaiian community. We are most fortunate to have the opportunity to conduct observations from this mountain. NM also wants to acknowledge that as the University of Victoria affiliates we are visitors on the traditional territory of the Coast Salish people and we thank the WS'ANEC' (Saanich), Lkwungen (Songhees) and Wyomilth (Esquimalt) peoples for an opportunity to work and reside in their lands.

REFERENCES

- Abgrall H., Roueff E., Drira I., 2000, *A&AS*, 141, 297
 Black, J. H., 1987, *ASSL*, 134, 731
 Centurión, M., Molaro, P., Vladilo, G., Péroux, C., Levshakov, S. A., D'Odorico, V., 2003, *A&A*, 403, 55
 de la Varga, A., Reimers, D., Tytler, D., Barlow, T., Burles, S., 2000, *A&A*, 363, 69
 Dessauges-Zavadsky, M., Péroux, C., Kim, T.-S., D'Odorico, S., McMahon, R. G., 2003, *MNRAS*, 345, 447
 Dessauges-Zavadsky, M., Calura, F., Prochaska, J. X., D'Odorico, S., Matteucci, F., 2004, *A&A*, 416, 79
 Dessauges-Zavadsky, M., Prochaska, J. X., D'Odorico, S., Calura, F., Matteucci, F., 2006, *A&A*, 445, 93
 Dessauges-Zavadsky, M., Ellison, S. L., Murphy, M. T., 2009 *MNRAS*, 396, L61
 D'Odorico, V., 2007, *A&A*, 470, 523
 Erb, D. K., Shapley, A. E., Pettini, M., Steidel, C. C., Reddy, N. A., Adelberger, K. L., 2006, *ApJ*, 644, 813
 Ellison, S. L., 2006, *MNRAS*, 368, 335
 Ellison, S. L., Hennawi, J. F., Martin, C. L., Sommer-Larsen, J., 2007, *MNRAS*, 378, 801
 Ellison, S. L., Kewley, L. J., & Mallén-Ornelas, G., 2005, *MNRAS*, 357, 354
 Ellison, S. L., Mallen-Ornelas, G., & Sawicki, M., 2003, *ApJ*, 589, 709
 Ellison, S. L., Murphy, M. T., Dessauges-Zavadsky, M., 2009, *MNRAS*, 392, 998
 Ellison, S. L., Prochaska, J. X., Hennawi, J., Lopez, S., Usher, C. G., Wolfe, A. M., Russell, D. M., Benn, C. R., 2010, *MNRAS*, in press
 Ferland G. J., Korista K. T., Verner D. A., Ferguson J. W., Kingdon J. B., Verner E. M., 1998, *PASP*, 110, 761
 Field, G. B., Goldsmith, D. W., Habing, H. J., 1969, *ApJ*, 155, L149
 Fox, A. J., Petitjean, P., Ledoux, C., Srianand, R., 2007, *ApJ*, 668, L15
 Haardt, F., Madau, P., 1996, *ApJ*, 461, 20
 Henry, R. B. C., Prochaska, J. X., 2007, *PASP*, 119, 962
 Herbert-Fort, S., Prochaska, J. X., Dessauges-Zavadsky, M., Ellison, S. L., Howk, J. C., Wolfe, A. M., Prochter, G. E., 2006, *PASP*, 118, 1077
 Howk, J.C., & Sembach, K.R. 1999, *ApJ*, 523, L141
 Grevesse N., Asplund M., Sauval A. J., 2007, *SSRv*, 130, 105
 Izotov, Y., Schaerer, D., Charbonnel, C., 2001, *ApJ*, 549, 878
 Kanekar, N.; Ghosh, T.; Chengalur, J. N., 2001, *A&A*, 373, 394
 Kanekar, N., Subrahmanyam, R., Ellison, S. L., Lane, W. M., Chengalur, J. N., 2006, *MNRAS*, 370, L46
 Kaplan, K. F., Prochaska, J. X., Herbert-Fort, S., Ellison, S. L., Dessauges-Zavadsky, M., 2010, *PASP*, in press.
 Krumholz, M. R., McKee, C. F., Tumlinson, J., 2009, *ApJ*, 693, 216
 Leboutteiller, V., Kunth, D., Thuan, T. X., Desert, J. M., 2009, *A&A*, 494, 915
 Lehner, N., Howk, J. C., Prochaska, J. X., Wolfe, A. M., 2008, *MNRAS*, 390, 2
 Maiolino, R., et al., 2008, *A&A*, 488, 463
 Malec, A. L., et al., 2010, *MNRAS*, 403, 1541.
 Meiring, J. D., Lauroesch, J. T., Kulkarni, V. P., Peroux, C., Khare, P., York, D. G., Crotts, A. P. S., 2007, *MNRAS*, 376, 557
 Meiring, J. D., Kulkarni, V. P., Lauroesch, J. T., Peroux, C., Khare, P., York, D. G., Crotts, A. P. S., 2008, *MNRAS*, 384, 1015
 Narayanan A., Misawa T., Charlton J. C., Ganguly R., 2006, *AJ*, 132, 2099
 Narayanan A., Charlton J. C., Misawa T., Green R. E., Kim T.-S., 2008, *ApJ*, 689, 782
 Noterdaeme, P., Ledoux, C., Petitjean, P., Srianand, R., 2008, *A&A*, 481, 327
 O'Meara, J. M., Prochaska, J. X., Burles, S., Prochter, G. Bernstein, R. A., Burgess, K. M., 2007, *ApJ*, 656, 666
 Pagel B. E. J., 1987, *Nucleosynthesis and chemical evolution of galaxies*. Cambridge University Press, UK.
 Péroux, C., Dessauges-Zavadsky, M., D'Odorico, S., Kim, T.-S., McMahon, R., 2003, *MNRAS*, 345, 480
 Péroux, C., Meiring, J. D., Kulkarni, V. P., Ferlet, R., Khare, P., Lauroesch, J. T., Vladilo, G., York, D. G., 2006, *MNRAS*, 372, 369
 Peroux, C., Dessauges-Zavadsky, M., D'Odorico, S., Kim, T.-S., McMahon, R. G., 2007, *MNRAS*, 382, 177
 Peroux, C., Meiring, J. D., Kulkarni, V. P., Khare, P., Lauroesch, J. T., Vladilo, G., York, D. G., 2008, *MNRAS*, 386, 2209
 Petitjean, P., Ledoux, C., Srianand, R., 2008, *A&A*, 480, 349
 Pettini, M., Ellison, S. L., Bergeron, J., Petitjean, P., 2002, *A&A*, 391, 21
 Pettini, M., Zych, B. J., Steidel, C. C., Chaffee, F. H., 2008, *MNRAS*, 385, 2011
 Pottasch, S. R., Wesselius, P. R., van Duinen, R. J., 1979, *A&A*, 74, L15
 Prochaska et al., 2007a, *ApJS*, 168, 231
 Prochaska J. X., Gawiser E., Wolfe A. M., Cooke J., Gelino D., 2003, *ApJS*, 147, 227
 Prochaska, J. X., Henry, R., O'Meara, J., Tytler, D., Wolfe, A., Kirkman, D., Lubin, D., Suzuki, N., 2002a, *PASP*, 114, 933
 Prochaska, J. X., Howk, J. C., O'Meara, J. M., Tytler, D., Wolfe, A. M., Kirkman, D., Lubin, D., Suzuki, N., 2002b, *ApJ*, 571, 693
 Prochaska, J. X., O'Meara, J. M., Herbert-Fort, S., Burles, S., Prochter, G. E., Bernstein, R. A., 2006, *ApJ*, 648, L97
 Prochaska, J. X., & Wolfe, A. M. 2002, *ApJ*, 566, 68
 Prochaska, J. X., Wolfe, A. M., Howk, J. C., Gawiser, E., Burles, S. M., Cooke, J., 2007b, *ApJS*, 171, 29
 Quast, R., Reimers, D., Baade, R., 2008, *A&A*, 477, 443
 Reimers, D., Baade, R., Quast, R., Levshakov, S. A., 2003, *A&A*, 410, 785
 Richter, P., Ledoux, C., Petitjean, P., Bergeron, J., 2005, *A&A*, 440, 819
 Schaye, J., 2001, *ApJL*, 562, L95
 Spitzer, L., & Jenkins, E. B., 1975, *ARA&A*, 13, 133
 Srianand R., Noterdaeme P., Ledoux C., Petitjean P., 2008, *A&A*, 482, L39
 Varshalovich D. A., Ivanchik A. V., Petitjean P., Srianand R., Ledoux C., 2001, *AstL*, 27, 683
 Viegas, S.M. 1995, *MNRAS*, 276, 268
 Vladilo, G., Centurion, M., Bonifacio, P., Howk, J. C., 2001, *ApJ*, 557, 1007
 Wolfe A. M., Prochaska J. X., 2000, *ApJ*, 545, 603
 Wolfe, A., Gawiser, E., & Prochaska, J. X., 2003, *ApJ*, 593, 235
 Wolfe, A. M., Gawiser, E., & Prochaska, J. X., 2005, *ARA&A*, 43, 861
 Wolfe, A. M., Prochaska, J. X., Jorgenson, R. A., Rafelski, M., 2008, *ApJ*, 681, 881
 Wright, E. L., 1991, *ApJ*, 381, 200
 York, B. A., Kanekar, N., Ellison, S. L., Pettini, M., 2007, *MNRAS*, 382, 53

APPENDIX A: EXTENDED ELEMENT STUDY IN CLOUDY

Figures A1 and A2 show the results of the Cloudy modeling described in Section 5 for a further six elements commonly observed in DLAs. These are presented here for completeness, but we note that these corrections are not generally applicable to the sub-DLA or DLA population as they are modelled for the particular parameters of J2123–0050.

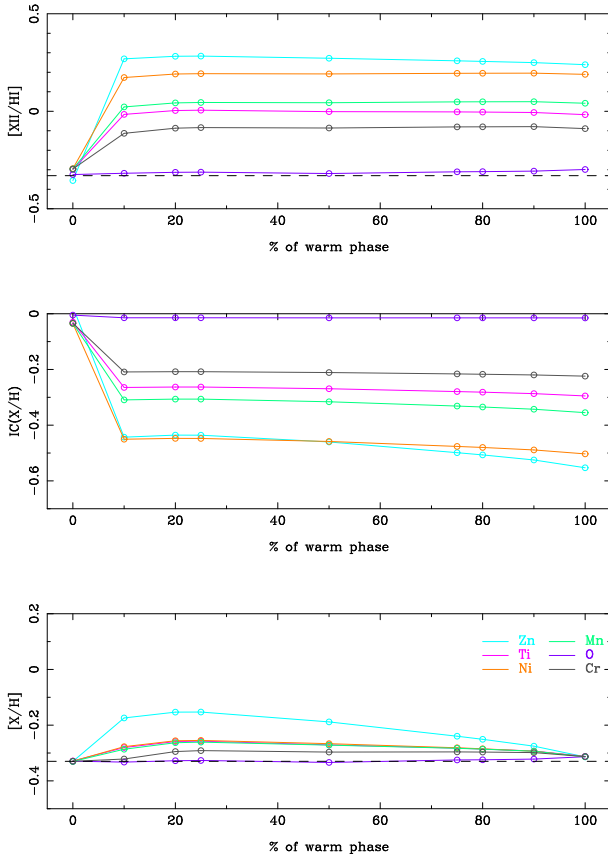


Figure A1. Ionization corrections for the theoretically modeled medium with $[M/H] = -0.33$. The ionic abundances ‘measured’ from the Cloudy models are presented in the top panel for different elemental species commonly measured in DLAs and sub-DLAs. The ionization corrections are given in the middle panel, and the corrected abundances are shown in the bottom panel. The black horizontal line represents the input metallicity of $[M/H] = -0.33$. The single-phase based corrections recover the metallicity of the clouds to within ~ 0.15 dex.

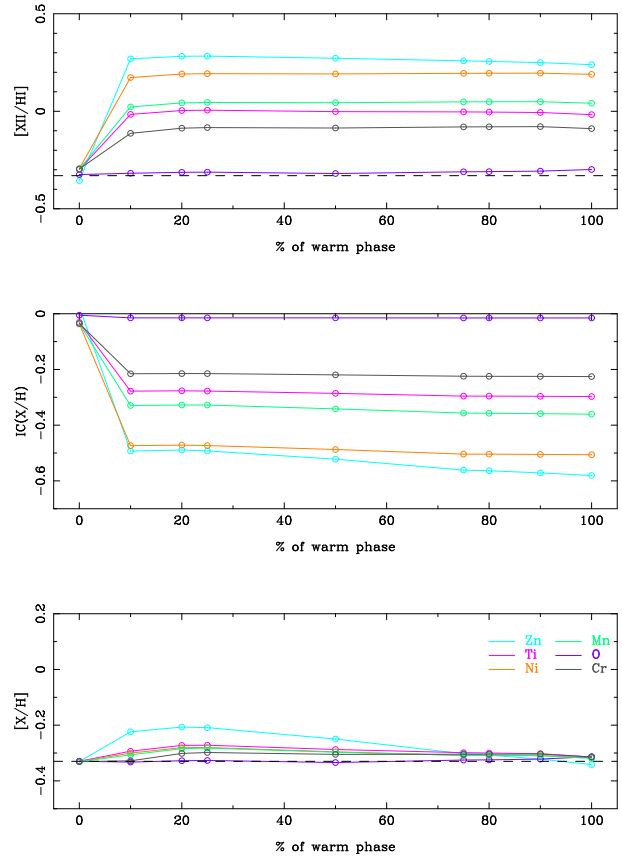


Figure A2. Same as in Figure A1, but for an assumed metallicity of $[M/H] = [Fe II/H I]$.